OXFORD

SOT | Society of Toxicology
www.toxsci.oxfordjournals.org

TOXICOLOGICAL SCIENCES, 169(1), 2019, 84–94

doi: 10.1093/toxsci/kfz028
Advance Access Publication Date: January 31, 2019
Research Article

Metabolomic Responses to Manganese Dose in SH-SY5Y Human Neuroblastoma Cells

Jolyn Fernandes, Joshua D. Chandler, Ken H. Liu, Karan Uppal, Li Hao, Xin Hu, Young-Mi Go,[1] and Dean P. Jones[1]

Division of Pulmonary, Allergy, Critical Care and Sleep Medicine, Department of Medicine, Emory University, Atlanta, Georgia 30322

[1]To whom correspondence should be addressed at Division of Pulmonary, Allergy, Critical Care and Sleep Medicine, Department of Medicine, Emory University, 205P Whitehead Biomedical Research Building, 615 Michael Street, Atlanta, GA 30322. Fax: 404-712-2974. E-mail: ygo@emory.edu.

ABSTRACT

Manganese (Mn)-associated neurotoxicity has been well recognized. However, Mn is also an essential nutrient to maintain physiological function. Our previous study of human neuroblastoma SH-SY5Y cells showed that Mn treatment comparable to physiological and toxicological concentrations in human brain resulted in different mitochondrial responses, yet cellular metabolic responses associated with such different outcomes remain uncharacterized. Herein, SH-SY5Y cells were examined for metabolic responses discriminated by physiological and toxicological levels of Mn using high-resolution metabolomics (HRM). Before performing HRM, we examined Mn dose (from 0 to100 μM) and time effects on cell death. Although we did not observe any immediate cell death after 5 h exposure to any of the Mn concentrations assessed (0–100 μM), cell loss was present after a 24-h recovery period in cultures treated with Mn ≥ 50 μM. Exposure to Mn for 5 h resulted in a wide range of changes in cellular metabolism including amino acids (AA), neurotransmitters, energy, and fatty acids metabolism. Adaptive responses at 10 μM showed increases in neuroprotective AA metabolites (creatine, phosphocreatine, phosphoserine). A 5-h exposure to 100 μM Mn, a time before any cell death occurred, resulted in decreases in energy and fatty acid metabolites (hexose-1,6 bisphosphate, acyl carnitines). The results show that adjustments in AA metabolism occur in response to Mn that does not cause cell death while disruption in energy and fatty acid metabolism occur in response to Mn that results in subsequent cell death. The present study establishes utility for metabolomics analyses to discriminate adaptive and toxic molecular responses in a human *in vitro* cellular model that could be exploited in evaluation of Mn toxicity.

Key words: adaptive response; cell metabolomics; metabolic pathway; neurotoxicity.

Manganese (Mn) is an essential cofactor for the antioxidant enzyme, superoxide dismutase 2 (SOD2), and for enzymes in amino acid (AA) and neurotransmitter metabolism (Smith *et al.*, 2017; Takeda, 2003). Mn is also toxic in excess, however, and the increasing production and application of Mn-containing compounds (Aschner *et al.*, 2005; ATSDR, 2012; Finkelstein and Jerrett, 2007) has raised concern that environmental Mn could be an unrecognized contributor to neurologic disorders, neurotoxicity, and parkinsonian-like symptoms (Kornblith *et al.*, 2018; Lucchini *et al.*, 2017; Normandin and Hazell, 2002; Takeda, 2003). Although many studies have explored the mechanisms of Mn toxicity (Liccione and Maines, 1988; Liu *et al.*, 2013; Normandin and Hazell, 2002; O'Neal and Zheng, 2015; Sarkar *et al.*, 2018; Zhang *et al.*, 2004), limited information is available about adaptive responses which could function in opposition to toxicity. In principle, understanding adaptive responses could be useful to predict individuals at risk of toxicity from excess Mn exposure and/or to develop prevention and treatment strategies.

A recent study by Baker *et al.* utilized metabolomics to identify biological signatures of Mn exposure in Mn-exposed

subjects recruited from a Mn steel foundry (Baker *et al.*, 2017). This study showed that 9 mass spectral features classified individuals according to Mn exposure status in an occupational cohort, thereby establishing the utility of metabolomics for evaluation of Mn exposures in humans. This use did not attempt to distinguish adaptive and toxic responses to Mn, however, and the authors recognized challenges due to the bottleneck in identification of the metabolites and metabolic pathways in untargeted metabolomics analyses with mass spectrometry (Baker *et al.*, 2017). In the current study, we used high-resolution metabolomics (HRM) platform which enables measurement of metabolites in most metabolic pathways (Walker *et al.*, 2016). This complements the approach by Baker *et al.* and creates an opportunity for detailed examination of metabolic responses evaluated by abundance, annotation, and associated pathway within physiological as well as toxicologic conditions. HRM uses liquid chromatography coupled to ultra-high-resolution mass spectrometry (LC-HRMS) and advanced computational tools to measure changes in metabolites and associated pathways and functional networks. Applications to study adverse effects of metals, fungicides, herbicides, and other environmental agents (Go *et al.*, 2014a; Kumar *et al.*, 2015; Roede *et al.*, 2014; Walker *et al.*, 2016; Wang *et al.*, 2015) show evidence for both adaptive and maladaptive responses to exposure. Although discrimination between beneficial and toxic pathways can be difficult, HRM methods are attractive because adaptive pathway and toxic metabolic phenotypes in *in vitro* models could be translated to study human responses to environmental or occupational Mn exposures.

Although cell models cannot recapitulate *in vivo* cellular responses in brain, several studies show the utility of human neuroblastoma SH-SY5Y cells for study of mitochondrial dysfunction, such as that caused by environmental toxicants, Mn, and pesticides (de Oliveira *et al.*, 2017; Fernandes *et al.*, 2017; Oh *et al.*, 2016; Wang *et al.*, 2014; Zhang *et al.*, 2016). In a previous study, we calibrated cellular Mn contents in SH-SY5Y cells to achieve values comparable to those in human brain and found that Mn-stimulated mitochondrial respiration and H_2O_2 production in dose-dependent manners (Fernandes *et al.*, 2017). Importantly, the dose-response characteristics differed in that respiration declined at doses greater than 10 μM Mn while H_2O_2 production continued to increase at higher concentrations, which also resulted in subsequent cell death. The results indicate that detailed analysis of metabolic perturbations under these conditions could provide a basis to discriminate adaptive (conditions where cells subsequently survived) and toxic (conditions where cells subsequently died) responses to Mn dose. Therefore, in the present study using the Mn dose range calibrated in the previous study, we utilized HRM to characterize adaptive versus toxicological Mn-dependent metabolic signature. Such an approach provides a composite cellular effect and elucidates biological pathways that could reflect impending cell fate to either cell survival or cell death by Mn. The results suggest that HRM could be exploited to discriminate adaptive and adverse responses to Mn to improve detection and management of related toxicity in humans.

MATERIALS AND METHODS

Cell culture, Mn and/or creatine treatments, and cell harvesting

Human neuroblastoma cell line SH-SY5Y was obtained from the American Type Culture Collection (ATCC, Manassas, Virginia). Cells were cultured in Dulbecco's modified Eagle medium/Ham's F12 medium (1:1 mixture) with 10% FBS and supplemented with (penicillin/streptomycin) in a humidified incubator with 5% CO_2 at 37°C. At 80% confluency, cells were treated with Mn (0, 1, 5, 10, 50, and 100 μM as $MnCl_2$; Sigma-Aldrich, St. Louis, Missouri) in 0.5% FBS media for 5 h. Subsets of cells pretreated with creatine (Sigma-Aldrich, 1 mM for 18 h) followed by co-incubation with or without Mn (100 μM, 5 h) were analyzed for metabolomics. Cell viability was measured by Trypan Blue exclusion assay. To help overcome limitations of false discovery in HRM, 9 biological replicates were used for each of the six experimental Mn concentrations. Previously measured cellular Mn content at 5 h under these conditions were, respectively, for Mn dose (μM) and cellular Mn content (ng Mn/mg protein): 0, 6.4 ± 1.0; 1, 12.0 ± 0.7; 5, 12.7 ± 1.8; 10, 15.7 ± 1.1; 50, 36.8 ± 1.8; 100, 49.2 ± 0.5 (Fernandes *et al.*, 2017). Cells attached to the dish were carefully washed 3 times with ice-cold phosphate-buffered saline and then treated with 200 μl of HPLC grade water: acetonitrile (1:2) containing 14 stable isotope internal standards (Go *et al.*, 2015a; Soltow *et al.*, 2013) and frozen at −80°C prior to analysis by HRM.

High-resolution metabolomics

Cells extracts were analyzed as described previously (Fernandes *et al.*, 2018; Go *et al.*, 2014b; Liu *et al.*, 2016). Briefly, thawed extracts were incubated at 4°C for 30 min, centrifuged at 16 100 g for 10 min to remove protein and transferred to a refrigerated (4°C) autosampler for analysis. Samples were analyzed with three technical replicates using ultra-high-resolution mass spectrometry with hydrophilic interaction liquid chromatography (HILIC) [Accucore HILIC 100 × 2.1 mm columns]. Electrospray ionization was used in the positive ion mode on a Thermo Scientific Q-Exactive HF mass spectrometer (Thermo, Waltham, Massachusetts) operating with resolution set to 120 000 and scan range set to 85–1275 *m/z* (mass to charge) (Liu *et al.*, 2016; Soltow *et al.*, 2013). A 2% formic acid/acetonitrile gradient was used as described (Liu *et al.*, 2016). Injection volume was 10 μl and run time was 10 min. Instrument conditions were: spray voltage, 3500 (V); capillary temperature, 300°C; sheath gas flow, 45 (arbitrary units); auxillary gas flow, 25 (arbitrary units); spare gas flow, 1 (arbitrary units); max spray current, 100 (μA); probe heater temperature, 200°C.

Data extraction and metabolite annotation

Peak detection and alignment were performed using *apLCMS* (Yu *et al.*, 2009) with *xMSanalyzer* (Uppal *et al.*, 2013), to yield data with mass to charge (*m/z*), retention time (RT, s), and intensity (integrated ion intensity) for each mass spectral feature for all samples. The data for technical replicates were averaged and filtered to retain features present in at least 80% of samples, resulting in 6296 mass spectral features. Missing values were imputed by one-half of the lowest signal detected for that feature across all samples and data were $\log_2$ transformed and quantile normalized. Mass spectral results included metabolites with identities confirmed by ion dissociation mass spectrometry (MS/MS; Schymanski Level 1 or Level 2), metabolites with Schymanski Level 5 identification (Schymanski *et al.*, 2014), and unidentified signals (accurate mass, RT, intensity). The latter were retained to enable future data mining when such metabolites are identified (Uppal *et al.*, 2016), but in current analyses, features that did not have accurate mass match to known

metabolites were not included in interpretation. For simplicity, we refer to mass spectral features as metabolites.

Hierarchical cluster analysis (HCA)-heatmap and partial least square-discriminant analysis (PLS-DA)

To visualize distributions of associated features, color-coded heatmap with the 2-way HCA was performed using the *hclust* function in R. To identify discriminatory metabolites contributing most to separation according to Mn exposure, PLS-DA was performed using Metaboanalyst (Xia and Wishart, 2016) and PLSDA function in R package mixOmics (Rohart *et al.*, 2017). Discriminatory metabolites were selected based on the variable importance for projection (VIP) measure (Rohart *et al.*, 2017). Biological networks and top pathways were reconstructed based on *mummichog* version 1.0.5 (Li *et al.*, 2013).

Biostatistics and bioinformatics

All statistical analyses were performed in R version 3.2.3. For the metabolome-wide association study (MWAS) of Mn, the intensity data for each *m/z* feature was $\log_2$ transformed and scale normalized prior to testing for correlation with percent-scaled cellular Mn concentration using a linear regression model (lmreg, $P \leq 0.05$). Type 1 and Type 2 Manhattan plots, representing respectively, the $-\log_{10} p$ versus *m/z* and $-\log_{10} p$ versus RT, were used to visualize distributions of correlated mass spectral features according to physical and chemical properties. In this, the Type 1 plot provides information indicating distribution of molecular mass of correlated features while the Type 2 plot provides information concerning the polarity of the features (nonpolar metabolites have shorter RT). Thresholds are provided for $p \leq .05$ without adjustment for multiple comparisons and for $q \leq 0.05$ after correction for false discovery rate (FDR) (Benjamini and Hochberg, 1995). Because previous research showed that FDR correction protects against type 1 statistical error but results in type 2 statistical error (Go *et al.*, 2015b), we used a 2-step procedure to protect against both type 1 and type 2 error (Uppal *et al.*, 2016). In this, all features with $p \leq .05$ were selected to protect against type 2 error. These features, any of which could be correct associations, were then used with *Mummichog* (version 1.0.5) pathway enrichment analyses to test for pathways enriched in these features (Li *et al.*, 2013). In this, permutation testing with $p \leq .05$ identified pathways enriched in features that vary in association with Mn. *Mummichog* output provides associated metabolites at identity Level 5 using criteria of Schymanski *et al.* (2014). Identities of AAs and other common metabolites were confirmed based upon ion dissociation spectra relative to authentic standards (Schymanski Level 1) or databases (Schymanski Level 2). For other metabolites, xMSannotator (Uppal *et al.*, 2017) was used to assign confidence scores based upon Human Metabolomics DataBase (HMDB; Wishart *et al.*, 2013) or Kyoto Encyclopedia of Genes and Genomes (http://www.genome.jp/kegg/; last accessed February 16, 2019) (Kanehisa *et al.*, 2017) with 5 ppm tolerance. Additional manual curation was performed using Metlin Mass Spectrometry Database (Smith *et al.*, 2005).

RESULTS

Cell Viability Following Mn Treatment

In a previously published study, Mn content over a 7.6-fold range (6.4–49 ng Mn/mg protein) had dose-dependent effects on mitochondrial and cellular redox status and on mitochondrial respiration (Fernandes *et al.*, 2017). In the current study, using the same Mn doses, no cell death was observed at 5 h for any Mn concentration studied (0, 1, 5, 10, 50, and 100 μM $MnCl_2$) (Figure 1), but substantial cell death was observed after a 24-h recovery period in cells treated with 50 or 100 μM Mn for 5 h (Figure 1). This dose range also comprised Mn cellular content over physiological to toxicological Mn concentration observed in human brain (Fernandes *et al.*, 2017). Thus, we selected 5 h as a time point where metabolic differences associated with cellular Mn content could be measured without complications caused by rapidly changing Mn content, cell death, or long-term effects on cell proliferation.

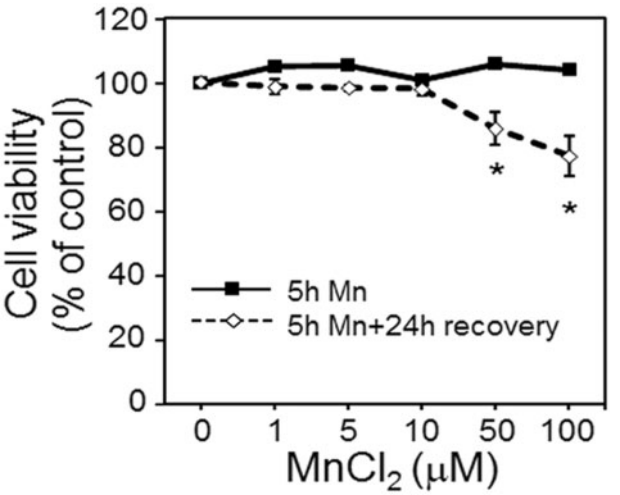

Figure 1. Cell viability at 5 h Mn treatment and 24 h post recovery. Viability of cells treated with 0, 1, 5, 10, 50, and 100 μM Mn concentration for 5 h is represented by the solid black line. At the end of 5 h, media including Mn was removed, cells washed 3 times and fresh growth media was added. Cell viability determined after 24 h recovery period is depicted by the dotted line. Data are expressed as the percentage of viable cells compared with no Mn treatment (mean ± SEM, $n = 3$ per treatment group).

Metabolomics Analysis

Metabolic differences associated with Mn were determined by a MWAS of cellular Mn using a linear regression model. MWAS showed that 4.5% (283/6296) of all metabolites varied in association with Mn at $p \leq .05$ (Figure 2). A complete list of the associated 283 metabolites is provided in Supplementary Table 1. Of these, a majority (66%, 188) decreased in abundance with increasing Mn while the remainder (34%, 95) increased with Mn. Of the 283 metabolites, majority (73%, 206) had *m/z* less than 400 (Figure 2A), and most were hydrophilic (Figure 2B). Application of Benjamini and Hochberg (BH) approach (Benjamini and Hochberg, 1995) to assess FDR showed that only a match to a diglyceride (*m/z* 564.4619, RT 79 s; DG 12: 0/17: 2; Pearson correlation, −0.6) was associated at FDR ≤ 0.05. Because this feature decreased with increasing Mn and has multiple isobaric matches, we did not consider this useful to mechanistic understanding and did not examine this further.

To gain additional understanding of metabolite associations with Mn, we performed 2-way hierarchical cluster analysis (HCA). The results showed 2 major clusters of samples (top dendrogram) with Cluster 1 including cells dosed with 0–10 μM and Cluster 2 including cells dosed at 50 or 100 μM (Figure 3A). These groupings corresponded to Mn treatments that did not cause cell death (0 – 10 μM) as compared with those causing cell death after 24 h (see Figure 1). Pathway enrichment analysis with all

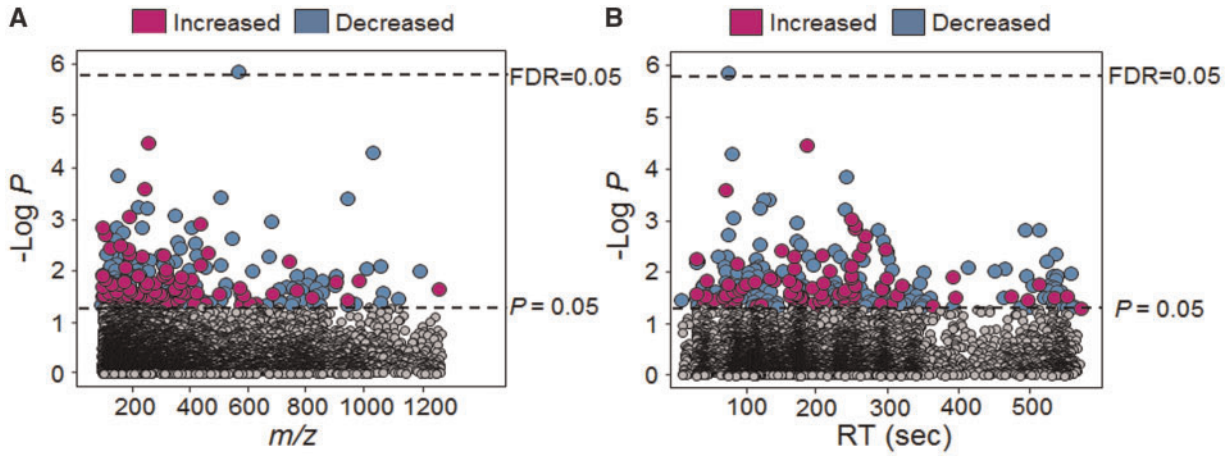

Figure 2. Metabolome-wide association study (MWAS) of dose-dependent cellular Mn in human SH-SY5Y cells. A, Type 1 Manhattan plot depicted by –log *P* against *m/z* (mass to charge) is plotted showing 283 discriminatory metabolites at *p*-value .05 threshold represented by bottom dotted line and at FDR 0.05 represented by top dotted line. B, Type 2 Manhattan plot depicted by –log *P* against RT (retention time, sec). Magenta circles represent features that were increased and the blue circles represent the features that were decreased with increasing cellular Mn accumulation. The list of *m/z* and RT along with *p*-value for the entire 283 metabolites is provided in Supplementary Table 1 ($n = 9$ per treatment group).

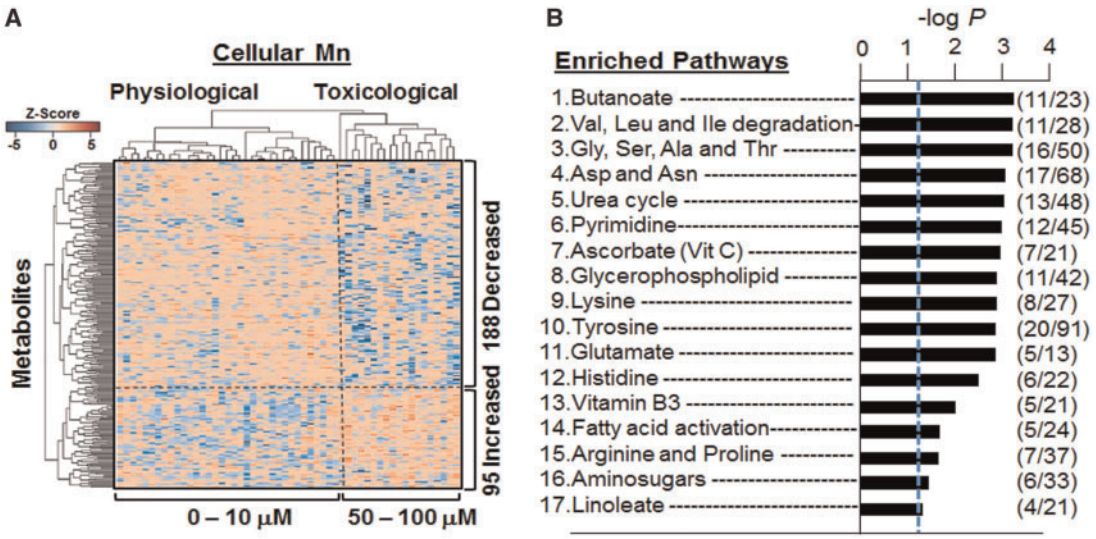

Figure 3. Hierarchal clustering and pathway enrichment analysis. A, Supervised hierarchal clustering of the 283 discriminatory metabolites clustered into 2 groups representing physiological and toxicological cellular Mn concentration is marked by a vertical dotted line. A total of 188 metabolites decreased (blue) and 95 metabolites increased (red) with increasing Mn cellular accumulation and is depicted by the horizontal dotted line. B, Enriched metabolic pathways using the 283 discriminatory features with cellular Mn concentration is demonstrated. A total of 17 significantly affected pathways are shown with –log *P* ($p < .05$) and comprising of ≥4 metabolites per pathway. Number of features that matched in the pathways are depicted as overlap/total features ($n = 9$ per treatment group).

283 metabolites showed that 17 pathways were enriched in metabolites that varied with Mn (Figure 3B). These included 8 AA pathways and the urea cycle, indicating a substantial effect on central cell processes linked to cell maintenance and/or proliferation. Other pathways were linked to energy metabolism (niacin and niacinamide), nucleoside metabolism (pyrimidine), carbohydrates (amino sugars), and lipid metabolism (butanoate, linoleate, and glycophospholipids) (Figure 3B). Results show that variations in response to cellular Mn content include widespread effects on cell metabolism.

Metabolites and Metabolic Pathways Altered by Mn

We performed PLS-DA analysis on the 283 metabolites that varied with Mn to determine the top ranked metabolites discriminating groups according to Mn content. The score plot showed separation according to Mn dose in principal component 1 (PC1) and little additional separation by PC2 (Figure 4A). The VIP score identified the top 30 contributing metabolites (Figure 4B). These included dihydrolipoamide, a critical coenzyme for mitochondrial respiratory function, along with an acyl-CoA, creatine, GMP, and CTP, all of which support the interpretation that Mn has major effects on energy metabolism. The top metabolites also included the antioxidant, GSH, and 6-phosphogluconate, an important precursor for NADPH supply. Other top metabolites included the neurotransmitter, γ-aminobutyric acid (GABA), and related metabolites (butanoate), and putrescine, a regulator of the neurotransmitter activity.

Detailed examination of the directionality of variation with Mn showed that glutamate and *N*-acetylglutamate semialdehyde had positive associations with Mn while other AAs

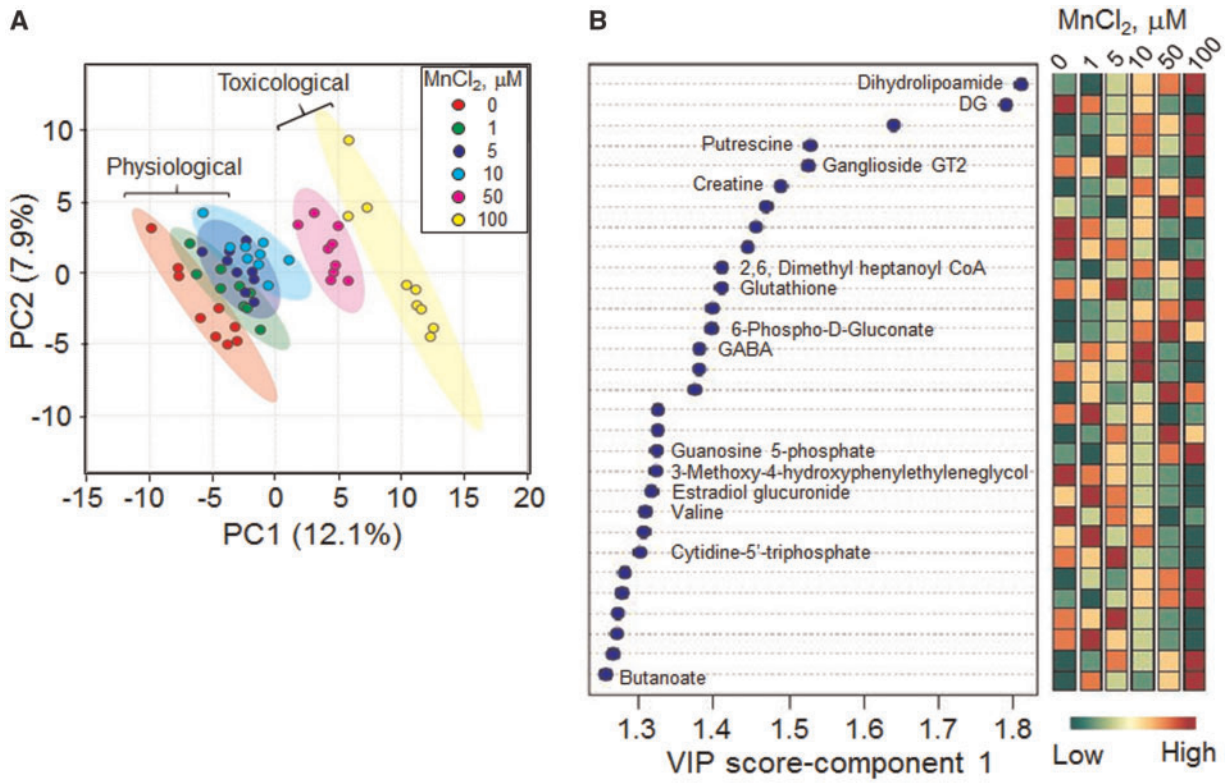

Figure 4. PLS-DA and the resultant top 30 discriminatory metabolic features contributing to the Mn dose-dependent separation. A, PLS-DA score plot for high-resolution metabolomics data resulting in a Mn dose-dependent separation is along principal component 1 (PC1–12.1%). B, The top 30 discriminatory metabolic features contributing to the separation listed from top to bottom is shown with their VIP scores (variable importance in projection scores) and changes in intensity at each Mn dose. The metabolite associated with the *m/z* features is marked as determined by Kegg ID.

including leucine/isoleucine, 4-imidazoleacetate, histidine, arginine, and valine had negative associations (Figs. 5A–D and Supplementar Figs. 1A–C). Metabolites functioning in energy and fatty acid metabolism that increased included dihydrolipoamide and hexose 1-phosphate while many others, such as phosphocholine, hexadecanoic acid, and tetradecanoyl carnitine, decreased in association with Mn (Figs. 5E–H and Supplementary Figure 1D). Neurotransmitters-related metabolites such as salsolinol-1-carboxylate, norepinephrine sulfate, and butanoate increased in association with Mn while GABA, adrenochrome, N4-acetylaminobutanal, *N*-methyl salsolinol and dopamine sulfate, decreased (Figs. 5I–L and Supplementar Figs. 1E–H).

Mn-Dependent Adaptive Metabolic Responses

Examination of the dose-response changes in metabolites revealed that some metabolites, such as hexadecanoic acid and GABA (Figure 5) and N4-acetylaminobutanal (Supplementary Figure 1), had relatively abrupt changes after 10 µM exposures. Because this could reflect differences between adaptive and toxic responses, we performed additional targeted comparisons to separate potentially beneficial changes under nontoxic conditions from changes occurring at concentrations which later caused cell death. In this, we selected 100 µM Mn as a toxic condition because this caused cell death after 24 h and 10 µM Mn as a nontoxic condition (see Figure 1). For each, we performed PLS-DA (Figs. 6A and 6C) and used metabolites with VIP scores >2 for pathway enrichment analysis. Results showed that the only pathways that differed between 10 µM Mn and control (0 µM Mn) were linked to regulation of Gly, Ser, Ala, and Thr AAs ($p = .008$). Metabolites with the top highest VIP score contributing to separation of these two groups included creatine, phosphocreatine, and phosphoserine (Figure 6B). In contrast, metabolites that differed for toxicologic Mn compared with control (100 µM Mn vs 0) were linked to hexose phosphorylation and fatty acid metabolism ($p = .02$ for both). Relevant metabolites with top VIP score included hexose 1,6-bisphosphate, hexadecenoyl carnitine, and octadecenoylcarnitine (Figure 6D). The results show that AA metabolism changes occur in response to Mn that does not cause cell death while energy and fatty acid metabolism changes occur in response to Mn that causes subsequent cell death.

Inhibition of Mn-Induced Toxic Response by Creatine

Cunha *et al.*, demonstrated protective effects of creatine on H_2O_2-induced toxicity in SH-SY5Y cells (Cunha *et al.*, 2016). On similar lines, we performed analysis in SH-SY5Y cells to determine whether creatine has protective roles in toxic Mn dose-caused alterations in energy and neurotransmitter metabolites using HRM. Results showed that cells pretreated with creatine (1 mM, 18 h) prior to Mn exposure (100 µM, 5 h) showed elevation of cellular creatine level (Supplementary Figure 2A) and blocked Mn-increased dihydrolipoamide, glutamate, and salsolinol carboxylate levels ($^{\#}p < .05$, Supplementary Figs. 2B–D). Energy metabolite such as hexose-1,6 bisphosphate showed a partial rescue in Mn-decreased abundance (Supplementary Figure 2E) with creatine supplement.

DISCUSSION

The present study shows that in a cell model of Mn toxicity, metabolic responses to nontoxic Mn exposure differ from

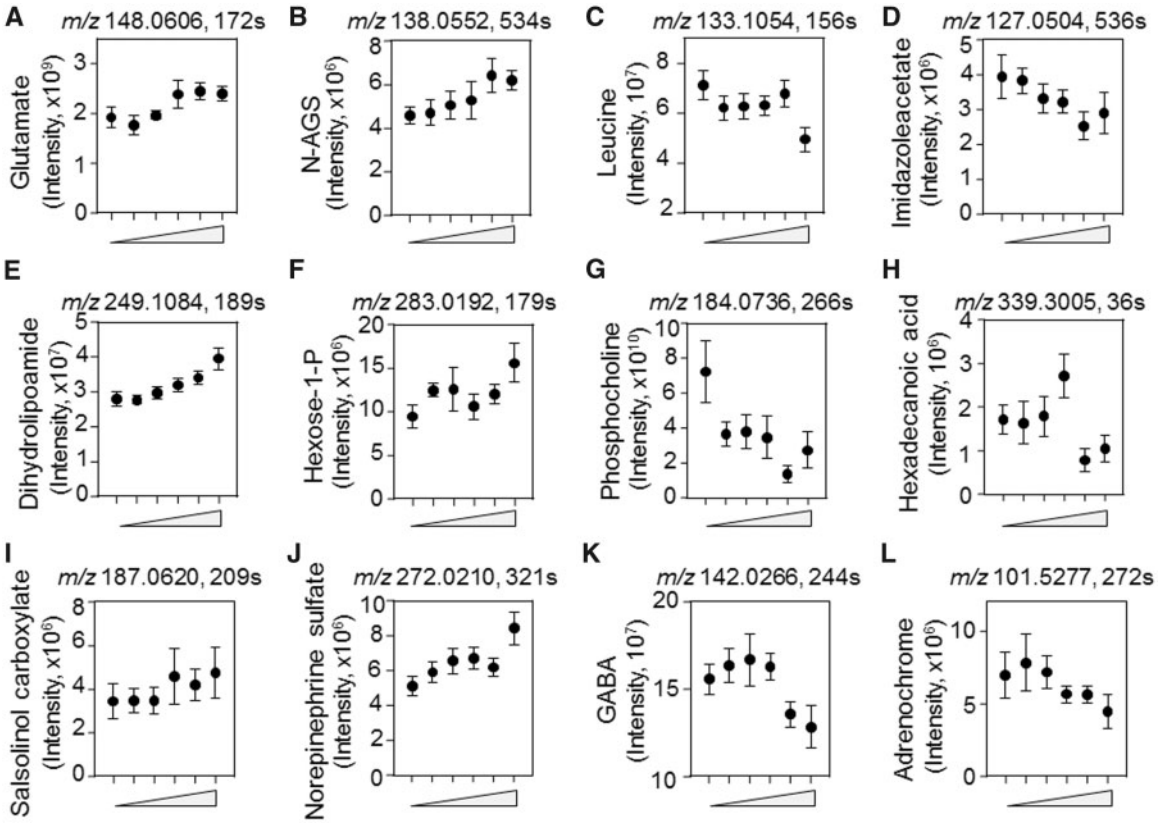

Figure 5. Key discriminatory metabolites plotted from the significantly enriched metabolic pathways altered by dose-dependent Mn concentration. A–L, The raw intensity of the representative metabolites with respect to Mn concentration (from left to right, 0, 1, 5, 10, 50, 100 μM) is plotted. Metabolites such as glutamate (A) *N*-acetyl glutamate semialdehyde (B), leucine/isoleucine (C), and 4-imidazoleacetate (D) from the amino acid pathway; dihydrolipoamide (E), hexose 1-phosphate (F), phosphocholine (G), and hexadecanoic acid (H) from energy metabolism; and salsolinol-1-carboxylate (I), sulfate derivative of norepinephrine (J), GABA (K), and adrenochrome (L) from the neurotransmitter pathway. The raw intensity for additional metabolites altered by Mn from these pathways are plotted in Supplementary Figure 1. ($p < .05$, mean ± SEM, $n = 9$ per treatment group).

responses caused by toxic Mn exposure. Earlier research established that neurotoxicity of Mn is related to disruption of mitochondrial function (Fernandes *et al.*, 2017; Gavin *et al.*, 1992, 1995; Zhang *et al.*, 2004), and the present studies show that toxic levels of Mn altered energy and fatty acid metabolism. Nontoxic Mn also caused widespread changes to creatine and the energy homeostatic mechanisms, urea cycle, and AA metabolism and neurotransmitter metabolism. We interpret these latter effects to include adaptive responses to Mn which occur over a physiologic range for this essential nutrient. Discrimination of such adaptive responses and toxic responses could provide criteria to improve diagnosis and management of neurotoxicity from Mn exposure.

Mn impacted multiple lipid metabolic pathways, including glycerophospholipid metabolism, fatty acid activation, and linoleate metabolism (Figure 3). A decrease in long-chain acyl carnitines as potential early diagnostic markers for Parkinson's disease has been proposed (Saiki *et al.*, 2017). In the current study, long chain acyl carnitines such as hexadecenoyl carnitine and octadecenoyl carnitine decreased at the highest Mn concentration (Figure 6). Saturated fatty acids, such as hexadecanoic acid (palmitate), also decreased with Mn content. A similar decrease in palmitate was observed following Mn^{4+} injection in rat brain (Neth *et al.*, 2015). Together, the data show that Mn has a profound effect on lipid and fatty acid metabolism in SH-SY5Y human neuroblastoma cells and Mn is negatively correlated with the majority of fatty acid metabolites. These effects occurred in SH-SY5Y cells at 50 and 100 μM Mn exposures, concentrations causing decreased mitochondrial respiration (Fernandes *et al.*, 2017). Because increased mitochondrial H_2O_2 production also occurs under these conditions, the results suggest that bioenergetic failure could result as a consequence of oxidative stress, disruption of fatty acid metabolism, and impaired mitochondrial bioenergetics (Figure 7).

The results show that toxic Mn exposure also disrupts carbohydrate metabolism at a critical point in glycolysis. Specifically, glucose 1-phosphate increased while hexose 1,6 bisphosphate decreased with highest Mn concentration, suggesting a disruption in phosphofructokinase step. This is a Mn-containing enzyme required for subsequent generation of ATP from the glycolytic pathway (Jones *et al.*, 1972). This observation, along with the decrease in fatty acid metabolites, supports earlier research showing mitochondrial dysfunction and failure of energy utilization, neurotoxicity, and ultimate cell death at toxic Mn exposure levels (Figure 7).

Prior research in a Huntington's disease (HD) model using immortalized mouse striatal neurons, established the utility of metabolomics to understand functional response to Mn (Kumar *et al.*, 2015), and the present study extends this use to provide potential metabolic signatures to discriminate Mn toxicity from adaptive responses. In the study of the HD mouse cell line, responses to Mn supported the hypothesis that changes in energetic processes underlie the pathobiology of both Mn neurotoxicity and HD (Kumar *et al.*, 2015). The results show metabolic

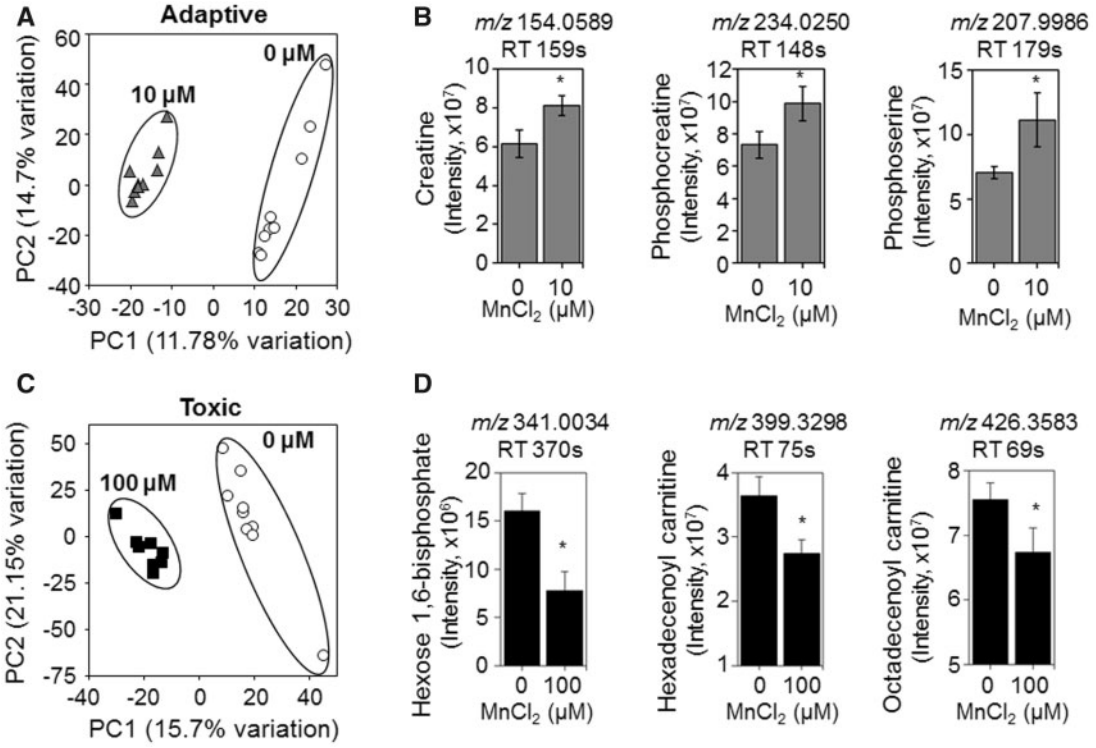

Figure 6. Metabolites and metabolic pathways representative of adaptive versus toxicological Mn content. A, PLS-DA score plot shows separation between control and 10 μM Mn-treated groups along principal component 1 and 2 which account for a 26.48% of the total variation for adaptive Mn concentration. B, Representative metabolites accounting for this separation including creatine, phosphocreatine, and phosphoserine are shown with bar graphs. C, PLS-DA score plot shows separation between control and 100 μM Mn-treated groups along principal component 1 and 2 which account for 36.85% of the total variation for toxicological Mn concentration. D, Representative metabolites accounting for this separation including hexose 1,6-bisphosphate, hexadecenoyl carnitine and octadecenoyl carnitine shown with bar graphs (mean ± SEM, $n = 9$ per treatment group). *$p < .05$.

responses due to Mn, and combined with the present results, show that widespread metabolic responses occur over a range including deficiency to the upper limit for the nutritional requirement. Recognition of this response is important for evaluation of environmental and occupational toxicity from Mn because of the natural and anthropogenic sources of exposures in humans (Howe *et al.*, 2004). Further, the reversibility of some of the neurobehavioral effects in Mn-exposed individuals (Bouchard *et al.*, 2007) supports the value to improved delineation of neurotoxic and adaptive metabolic responses observed for energy metabolism, urea cycle, and AA metabolism and neurotransmitter metabolism.

In the current study, Mn at a physiological dosage when compared with control caused an increase in creatine and phosphocreatine levels demonstrating a protective and adaptive response in the current human neuroblastoma model. Creatine when phosphorylated to phosphocreatine, is used to replenish ATP stores in the cytoplasm. Creatine and phosphocreatine are shown to counteract apoptosis, excitotoxicity, and oxidative stress (Lawler *et al.*, 2002; O'Gorman *et al.*, 1997; Xu *et al.*, 1996). Creatine has also been reported to be a neuroprotective agent (Genius *et al.*, 2012; Klein and Ferrante, 2007) and its therapeutic use has been proposed for neurological disorder such as Parkinson's, Alzheimer's, ALS, HD, and mitochondrial diseases (Cunha *et al.*, 2016; Klein and Ferrante, 2007; Klivenyi *et al.*, 1999; Lin *et al.*, 2013; Rae and Broer, 2015; Stevens *et al.*, 2014). Consistently, we also found a protective effect of creatine on toxicological Mn dose-induced metabolic response in SH-SY5Y cells (see Supplementary Figure 2) suggesting that cellular creatine level plays an important role in metabolic responses to Mn doses. Additional experiments with multiple creatine doses, Mn dose, and time course will be needed to better understand related mechanisms.

In the current study, Mn at a physiological dosage when compared with control demonstrated increase in phosphoserine reflecting an adaptive protective response potentially against stress in the current human neuroblastoma model. A small-molecule screening also demonstrated phosphoserine as a neurogenic enhancer with group III metabotropic glutamate receptor 4 as its target, which plays an important role in anxiety, depression, and stress disorders (Swanson *et al.*, 2005). Phosphoserine is also shown to promote neuronal differentiation of human embryonic stem cell-derived neural stem cells, and has been suggested to be of potential therapeutic value for regenerative medicine (Saxe *et al.*, 2007). Together, the results suggest that changes in creatine, phosphocreatine, and phosphoserine at nontoxic Mn exposures occur as part of adaptive response and that further efforts are warranted to evaluate therapeutic value of these metabolites in Mn toxicity.

Disruption of AA metabolism and urea cycle dysfunction has been implicated in a number of neurological disorders (Gropman *et al.*, 2007). Mn is directly important in this pathway because conversion of arginine to urea and ornithine is catalyzed by arginase, a Mn-dependent enzyme. We previously found that Mn altered putrescine and other polyamines derived from ornithine (Fernandes *et al.*, 2018). In addition, Mn decreased arginine and increased *N*-acetyl-L-glutamate 5-semialdehyde, the second to last step in ornithine biosynthesis. Low levels of arginine previously were associated with major depressive disorders (Ali-Sisto *et al.*, 2018). Decline in branched chain

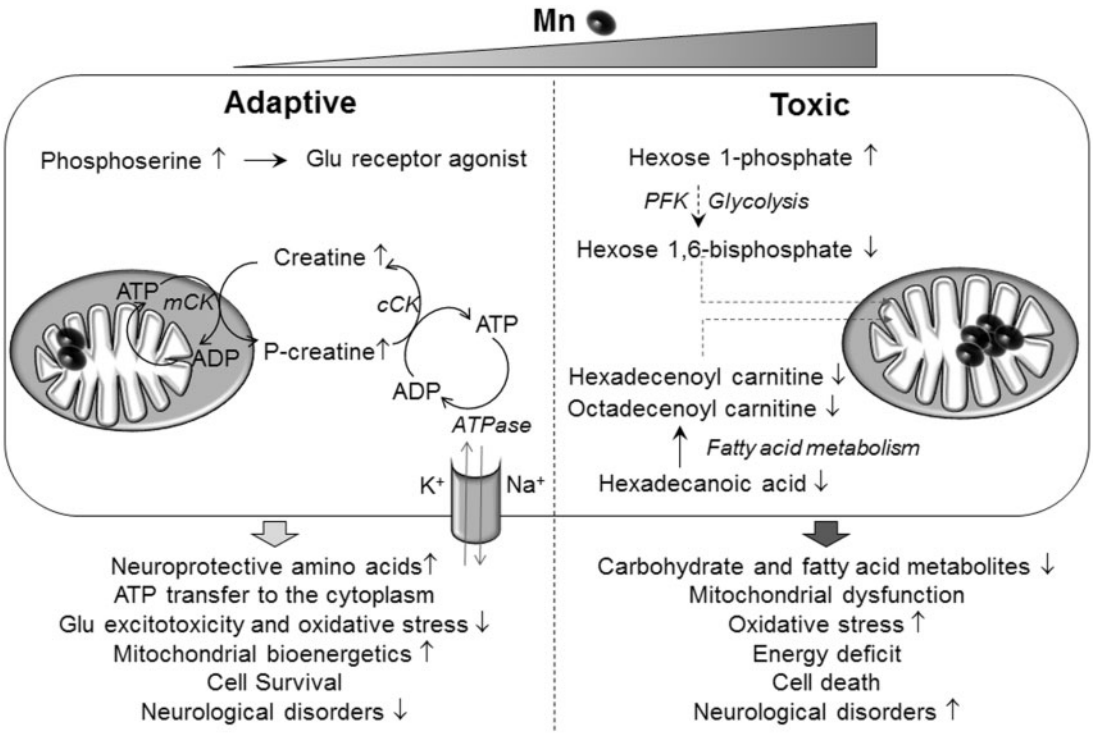

Figure 7. A proposed schematic diagram representing Mn-dependent adaptive and toxic cellular responses. Adaptive (left), human neuroblastoma cells (SH-SY5Y) exposed to physiological Mn stimulates adjustment in amino acid metabolism by increasing metabolites such as creatine, phosphocreatine, and phosphoserine. The creatine kinase enzyme (mCK), present in the mitochondrial inter membrane space generates phosphocreatine using creatine, and ATP generated in the mitochondria, while the cytoplasmic creatine kinase (cCK), regenerates ATP in the cytoplasm. Thus, providing a rapid supply of ATP that is used by ATP-dependent processes such as ATPase for Na^+ and K^+ pump or providing ADP supply for energy-generating processes such as glycolysis. Neuroprotective amines are known to prevent glutamate excitotoxicity, reduce oxidative stress, and enhance mitochondrial bioenergetics. Phosphoserine is a glutamate receptor agonist and promotes neuronal differentiation, thereby providing potential for regenerative medicine. These neuroprotective amines thus promote cell survival that could protect against neurological diseases. Toxic (right), cells exposed to toxic Mn disrupts energy and fatty acid metabolism by decreasing hexose 1,6 bisphosphate and acyl carnitine esters such as octadecenoyl carnitine and hexadecenoyl carnitine. Phosphofructokinase (PFK) is an important enzyme in glycolysis that generates hexose 1,6-bisphosphate and uses Mn as a cofactor. Decline in energy substrates used by the mitochondria could lead to mitochondrial dysfunction. Additionally accumulation of mitochondrial oxidative stress with toxic Mn could exacerbate mitochondrial dysfunction eventually resulting in cell death and inability to recover. This deleterious combination could eventually precipitate into Mn neurotoxicity and neurological disorders.

amino acids (BCAA) levels have also been found in the plasma following traumatic brain injury (Jeter *et al.*, 2013). BCAA are crucial to protein synthesis, degradation, and neurotransmitter synthesis and, in the current study, leucine/isoleucine and valine decreased with increasing Mn content (see Figs. 3, 5, and Supplementary Figure 1). BCAA supplementation is a nutritional strategy for treating diseases with protein degradation (Tamanna and Mahmood, 2014) and leads to improved outcome (Elkind *et al.*, 2015).

In catecholamine metabolism, tetrahydrobiopterin, an essential cofactor of tyrosine hydroxylase and dopamine synthesis, decreased in a Mn dose-dependent manner. This agreed with an earlier finding that intrastriatal injection of manganese chloride in rats led to decline in total biopterin levels (Lista *et al.*, 1986). Also, cerebrospinal fluid (CSF) from Parkinsonian patients contains half the amount of tetrahydrobiopterin as compared with age-matched controls (Lovenberg *et al.*, 1979; Williams *et al.*, 1980). Our data also showed that Mn decreased dopamine-O-sulfate in a dose-dependent manner; this is the predominant circulating form of dopamine in the plasma (Kuchel and Kuchel, 1991). Mn also caused a decline in adrenochrome, the oxidized form of epinephrine, while increasing the sulfated derivative of norepinephrine. The downstream dopamine metabolite, salsolinol-1-carboxylate, was also increased by Mn; sasolinol and its metabolites are endogenous neurotoxins and considered a potential causative factor for Parkinsonism (Naoi *et al.*, 2002; Zhu *et al.*, 2008). Thus, the results indicate that Mn at concentrations below those causing mitochondrial dysfunction and cell death could alter catecholamine metabolism in ways that affect neuronal functions.

This interpretation is also supported by results on glutamatergic metabolism, another neurotransmitter pathway altered by Mn. Glutamate, the precursor molecule increased, suggesting Mn tips the balance toward more excitatory phenotype. Glutamate-induced excitotoxicity-related neuronal cell death has been observed in multiple neurodegenerative diseases such as ALS (Shaw *et al.*, 2001) and Alzheimer's disease (Schubert and Piasecki, 2001). In contrast, increasing cellular Mn led to a decline in N4-acetylaminobutanal and 4-aminobutanoate (GABA), an inhibitory neurotransmitter. GABAergic/glutamatergic imbalance has been observed in a number of neurological disorders such as epilepsies (Treiman, 2001) and autism (El-Ansary and Al-Ayadhi, 2014). Together with previous findings of effects of Mn on polyamine metabolism, the present results showing effects of Mn on AA and neurotransmitter metabolism indicates that Mn could have subtle neurotoxic effects at concentrations below those causing disruption of mitochondrial energy metabolism and cell death.

Limitations of the current study are recognized. First, the current Mn exposure results are based on the use of one form of

Mn ($MnCl_2$). Mn interacts with oxygen, sulfur, and chlorine all of which are found in the environment (ATSDR, 2012) and hence the generalizability of results may be limited with different forms. Our previous study determined intracellular Mn concentration for each Mn treatment used in the current study and hence the current cellular results are associated with relevant Mn concentration in human brain (Fernandes *et al.*, 2017). Second, the studies were performed in SH-SY5Y cells, which is a human neuroblastoma cell line that differs from normal neurons. These cells show disruption in energy metabolism at Mn concentrations leading to cell death, but are also known to be highly glycolytic. Thus, additional studies of Mn-dependent effects are required in neuronal as well as other cell lines to support translation to more complex *in vivo* systems.

In conclusion, the current *in vitro* cellular metabolomics analyses shows that exposure of human SH-SY5Y neuroblastoma cells to Mn representing brain concentrations in the physiologic to pathologic range causes disruption of energy metabolism at concentrations causing cell death. Widespread metabolic effects were also observed at doses that did not cause cell death. These included changes in energy homeostatic systems which were interpreted to represent adaptive physiologic responses to variation in Mn. Additional changes in AA and neurotransmitter metabolism occurred at Mn concentrations that did not cause cell death; these reflected patterns observed with neurological disorders and suggest that metabolomics could be used to improve evaluation and management of environmental and occupational Mn toxicities.

SUPPLEMENTARY DATA

Supplementary data are available at *Toxicological Sciences* online.

DECLARATION OF CONFLICTING INTERESTS

The author(s) declared no potential conflicts of interest with respect to the research, authorship, and/or publication of this article.

ACKNOWLEDGMENTS

Drs Young-Mi Go and Dean P. Jones share equal senior authorship in this collaborative research. The authors thank ViLinh Tran for technical assistance with the mass spectrometer.

FUNDING

NIEHS grants R01 ES023485 (D.P.J. and Y.M.G.), R21 ES025632 (D.P.J. and Y.M.G.), P30 ES019776 (D.P.J.), and NIH S10 OD018006 (D.P.J.).

REFERENCES

Ali-Sisto, T., Tolmunen, T., Viinamaki, H., Mantyselka, P., Valkonen-Korhonen, M., Koivumaa-Honkanen, H., Honkalampi, K., Ruusunen, A., Nandania, J., Velagapudi, V., *et al.* (2018). Global arginine bioavailability ratio is decreased in patients with major depressive disorder. *J. Affect Disord.* **229,** 145–151.

Aschner, M., Erikson, K. M., and Dorman, D. C. (2005). Manganese dosimetry: Species differences and implications for neurotoxicity. *Crit. Rev. Toxicol.* **35,** 1–32.

ATSDR (2012). *Toxicological Profile for Manganese*. United States Department of Health and Human Services, Public Health Service, Agency for Toxic Substances and Disease Registry, Atlanta GA.

Baker, M. G., Simpson, C. D., Lin, Y. S., Shireman, L. M., and Seixas, N. (2017). The use of metabolomics to identify biological signatures of manganese exposure. *Annal. Work Exp. Health* **61,** 406–415.

Benjamini, Y., and Hochberg, Y. (1995). Controlling the false discovery rate: A practical and powerful approach to multiple testing. *J. Royal Statistical Soc.* **57,** 289–300.

Bouchard, M., Mergler, D., Baldwin, M., Panisset, M., Bowler, R., and Roels, H. A. (2007). Neurobehavioral functioning after cessation of manganese exposure: A follow-up after 14 years. *Am. J. Ind. Med.* **50,** 831–840.

Cunha, M. P., Lieberknecht, V., Ramos-Hryb, A. B., Olescowicz, G., Ludka, F. K., Tasca, C. I., Gabilan, N. H., and Rodrigues, A. L. (2016). Creatine affords protection against glutamate-induced nitrosative and oxidative stress. *Neurochem. Int.* **95,** 4–14.

de Oliveira, M. R., Peres, A., Ferreira, G. C., Schuck, P. F., Gama, C. S., and Bosco, S. M. D. (2017). Carnosic acid protects mitochondria of human neuroblastoma SH-SY5Y cells exposed to paraquat through activation of the Nrf2/HO-1 axis. *Mol. Neurobiol.* **54,** 5961–5972.

El-Ansary, A., and Al-Ayadhi, L. (2014). GABAergic/glutamatergic imbalance relative to excessive neuroinflammation in autism spectrum disorders. *J. Neuroinflammation* **11,** 189.

Elkind, J. A., Lim, M. M., Johnson, B. N., Palmer, C. P., Putnam, B. J., Kirschen, M. P., and Cohen, A. S. (2015). Efficacy, dosage, and duration of action of branched chain amino Acid therapy for traumatic brain injury. *Front Neurol.* **6,** 73.

Fernandes, J., Chandler, J. D., Liu, K. H., Uppal, K., Go, Y. M., and Jones, D. P. (2018). Putrescine as indicator of manganese neurotoxicity: Dose-response study in human SH-SY5Y cells. *Food Chem. Toxicol.* **116,** 272–280.

Fernandes, J., Hao, L., Bijli, K. M., Chandler, J. D., Orr, M., Hu, X., Jones, D. P., and Go, Y. M. (2017). From the cover: Manganese stimulates mitochondrial H_2O_2 production in SH-SY5Y human neuroblastoma cells over physiologic as well as toxicologic range. *Toxicol. Sci.* **155,** 213–223.

Finkelstein, M. M., and Jerrett, M. (2007). A study of the relationships between Parkinson's disease and markers of traffic-derived and environmental manganese air pollution in two Canadian cities. *Environ. Res.* **104,** 420–432.

Galvani, P., Fumagalli, P., and Santagostino, A. (1995). Vulnerability of mitochondrial complex I in PC12 cells exposed to manganese. *Eur. J. Pharmacol.* **293,** 377–383.

Gavin, C. E., Gunter, K. K., and Gunter, T. E. (1992). Mn2+ sequestration by mitochondria and inhibition of oxidative phosphorylation. *Toxicol. Appl. Pharmacol.* **115,** 1–5.

Genius, J., Geiger, J., Bender, A., Moller, H. J., Klopstock, T., and Rujescu, D. (2012). Creatine protects against excitoxicity in an in vitro model of neurodegeneration. *PLoS One* **7,** e30554.

Go, Y. M., Roede, J. R., Orr, M., Liang, Y., and Jones, D. P. (2014). Integrated redox proteomics and metabolomics of mitochondria to identify mechanisms of cd toxicity. *Toxicol. Sci.* **139,** 59–73.

Go, Y. M., Uppal, K., Walker, D. I., Tran, V., Dury, L., Strobel, F. H., Baubichon-Cortay, H., Pennell, K. D., Roede, J. R., and Jones, D. P. (2014b). Mitochondrial metabolomics using high-resolution Fourier-transform mass spectrometry. *Methods Mol. Biol.* **1198,** 43–73.

Go, Y. M., Walker, D. I., Liang, Y., Uppal, K., Soltow, Q. A., Tran, V., Strobel, F., Quyyumi, A. A., Ziegler, T. R., Pennell, K. D., *et al.* (2015). Reference standardization for mass spectrometry and high-resolution metabolomics applications to exposome research. *Toxicol. Sci.* **148,** 531–543.

Go, Y. M., Walker, D. I., Soltow, Q. A., Uppal, K., Wachtman, L. M., Strobel, F. H., Pennell, K., Promislow, D. E., and Jones, D. P. (2015). Metabolome-wide association study of phenylalanine in plasma of common marmosets. *Amino Acids* **47,** 589–601.

Gropman, A. L., Summar, M., and Leonard, J. V. (2007). Neurological implications of urea cycle disorders. *J. Inherit. Metab. Dis.* **30,** 865–879.

Howe, P., Malcolm, H., Dobson, S., World Health Organization, United Nations Environment Programme, Organisation, International Labour Organization, and Inter-Organization Programme for the Sound Management of Chemicals (2004). *Manganese and Its Compounds: Environmental Aspects*. World Health Organization, Geneva, Switzerland.

Jeter, C. B., Hergenroeder, G. W., Ward, N. H., 3rd, Moore, A. N., and Dash, P. K. (2013). Human mild traumatic brain injury decreases circulating branched-chain amino acids and their metabolite levels. *J. Neurotrauma* **30,** 671–679.

Jones, R., Dwek, R. A., and Walker, I. O. (1972). Magnetic resonance studies on manganese-activated phosphofructokinase. *Eur. J. Biochem.* **28,** 74–82.

Kanehisa, M., Furumichi, M., Tanabe, M., Sato, Y., and Morishima, K. (2017). KEGG: New perspectives on genomes, pathways, diseases and drugs. *Nucleic Acids Res.* **45,** D353–D361.

Klein, A. M., and Ferrante, R. J. (2007). The neuroprotective role of creatine. *Subcell Biochem.* **46,** 205–243.

Klivenyi, P., Ferrante, R. J., Matthews, R. T., Bogdanov, M. B., Klein, A. M., Andreassen, O. A., Mueller, G., Wermer, M., Kaddurah-Daouk, R., and Beal, M. F. (1999). Neuroprotective effects of creatine in a transgenic animal model of amyotrophic lateral sclerosis. *Nat. Med.* **5,** 347–350.

Kornblith, E. S., Casey, S. L., Lobdell, D. T., Colledge, M. A., and Bowler, R. M. (2018). Environmental exposure to manganese in air: Tremor, motor and cognitive symptom profiles. *Neurotoxicology*. **64**, 152–158.

Kuchel, O. G., and Kuchel, G. A. (1991). Peripheral dopamine in pathophysiology of hypertension. Interaction with aging and lifestyle. *Hypertension* **18,** 709–721.

Kumar, K. K., Goodwin, C. R., Uhouse, M. A., Bornhorst, J., Schwerdtle, T., Aschner, M., McLean, J. A., and Bowman, A. B. (2015). Untargeted metabolic profiling identifies interactions between Huntington's disease and neuronal manganese status. *Metallomics* **7,** 363–370.

Lawler, J. M., Barnes, W. S., Wu, G., Song, W., and Demaree, S. (2002). Direct antioxidant properties of creatine. *Biochem. Biophys. Res. Commun.* **290,** 47–52.

Li, S., Park, Y., Duraisingham, S., Strobel, F. H., Khan, N., Soltow, Q. A., Jones, D. P., and Pulendran, B. (2013). Predicting network activity from high throughput metabolomics. *PLoS Comput. Biol.* **9,** e1003123.

Liccione, J. J., and Maines, M. D. (1988). Selective vulnerability of glutathione metabolism and cellular defense mechanisms in rat striatum to manganese. *J. Pharmacol. Exp. Ther.* **247,** 156–161.

Lin, Y. S., Cheng, T. H., Chang, C. P., Chen, H. M., and Chern, Y. (2013). Enhancement of brain-type creatine kinase activity ameliorates neuronal deficits in Huntington's disease. *Biochim. Biophys. Acta*. **1832,** 742–753.

Lista, A., Abarca, J., Ramos, C., and Daniels, A. J. (1986). Rat striatal dopamine and tetrahydrobiopterin content following an intrastriatal injection of manganese chloride. *Life Sci.* **38,** 2121–2127.

Liu, K. H., Walker, D. I., Uppal, K., Tran, V., Rohrbeck, P., Mallon, T. M., and Jones, D. P. (2016). High-resolution metabolomics assessment of military personnel: Evaluating analytical strategies for chemical detection. *J. Occup. Environ. Med.* **58,** S53–S61.

Liu, Y., Barber, D. S., Zhang, P., and Liu, B. (2013). Complex II of the mitochondrial respiratory chain is the key mediator of divalent manganese-induced hydrogen peroxide production in microglia. *Toxicol. Sci.* **132,** 298–306.

Lovenberg, W., Levine, R. A., Robinson, D. S., Ebert, M., Williams, A. C., and Calne, D. B. (1979). Hydroxylase cofactor activity in cerebrospinal fluid of normal subjects and patients with Parkinson's disease. *Science* **204,** 624–626.

Lucchini, R., Placidi, D., Cagna, G., Fedrighi, C., Oppini, M., Peli, M., and Zoni, S. (2017). Manganese and developmental neurotoxicity. *Adv. Neurobiol.* **18,** 13–34.

Naoi, M., Maruyama, W., Akao, Y., and Yi, H. (2002). Dopamine-derived endogenous N-methyl-(R)-salsolinol: Its role in Parkinson's disease. *Neurotoxicol. Teratol.* **24,** 579–591.

Neth, K., Lucio, M., Walker, A., Zorn, J., Schmitt-Kopplin, P., and Michalke, B. (2015). Changes in brain metallome/metabolome pattern due to a single i.v. injection of manganese in rats. *PLoS One* **10,** e0138270.

Normandin, L., and Hazell, A. S. (2002). Manganese neurotoxicity: An update of pathophysiologic mechanisms. *Metab. Brain Dis.* **17,** 375–387.

O'Gorman, E., Beutner, G., Dolder, M., Koretsky, A. P., Brdiczka, D., and Wallimann, T. (1997). The role of creatine kinase in inhibition of mitochondrial permeability transition. *FEBS Lett.* **414,** 253–257.

O'Neal, S. L., and Zheng, W. (2015). Manganese toxicity upon overexposure: A decade in review. *Curr. Environ. Health Rep.* **2,** 315–328.

Oh, Y., Jeong, K., Kim, K., Lee, Y. S., Jeong, S., Kim, S. S., Yoon, K. S., Ha, J., Kang, I., and Choe, W. (2016). Cyclophilin B protects SH-SY5Y human neuroblastoma cells against MPP(+)-induced neurotoxicity via JNK pathway. *Biochem. Biophys. Res. Commun.* **478,** 1396–1402.

Rae, C. D., and Broer, S. (2015). Creatine as a booster for human brain function. How might it work? *Neurochem. Int.* **89,** 249–259.

Roede, J. R., Uppal, K., Park, Y., Tran, V., and Jones, D. P. (2014). Transcriptome-metabolome wide association study (TMWAS) of maneb and paraquat neurotoxicity reveals network level interactions in toxicologic mechanism. *Toxicol. Rep.* **1,** 435–444.

Rohart, F., Gautier, B., Singh, A., and Le Cao, K. A. (2017). mixOmics: An R package for 'omics feature selection and multiple data integration. *PLoS Comput. Biol.* **13,** e1005752.

Saiki, S., Hatano, T., Fujimaki, M., Ishikawa, K. I., Mori, A., Oji, Y., Okuzumi, A., Fukuhara, T., Koinuma, T., Imamichi, Y., *et al.* (2017). Decreased long-chain acylcarnitines from insufficient beta-oxidation as potential early diagnostic markers for Parkinson's disease. *Sci. Rep.* **7,** 7328.

Sarkar, S., Malovic, E., Harischandra, D. S., Ngwa, H. A., Ghosh, A., Hogan, C., Rokad, D., Zenitsky, G., Jin, H., Anantharam, V., *et al.* (2018). Manganese exposure induces neuroinflammation by impairing mitochondrial dynamics in astrocytes. *Neurotoxicology*. **64**, 204–218.

Saxe, J. P., Wu, H., Kelly, T. K., Phelps, M. E., Sun, Y. E., Kornblum, H. I., and Huang, J. (2007). A phenotypic small-molecule screen identifies an orphan ligand-receptor pair that regulates neural stem cell differentiation. *Chem. Biol.* **14,** 1019–1030.

Schubert, D., and Piasecki, D. (2001). Oxidative glutamate toxicity can be a component of the excitotoxicity cascade. *J. Neurosci.* **21,** 7455–7462.

Schymanski, E. L., Jeon, J., Gulde, R., Fenner, K., Ruff, M., Singer, H. P., and Hollender, J. (2014). Identifying small molecules via high resolution mass spectrometry: Communicating confidence. *Environ. Sci. Technol.* **48,** 2097–2098.

Shaw, C. E., al-Chalabi, A., and Leigh, N. (2001). Progress in the pathogenesis of amyotrophic lateral sclerosis. *Curr. Neurol. Neurosci. Rep.* **1,** 69–76.

Smith, C. A., O'Maille, G., Want, E. J., Qin, C., Trauger, S. A., Brandon, T. R., Custodio, D. E., Abagyan, R., and Siuzdak, G. (2005). METLIN: A metabolite mass spectral database. *Ther. Drug Monit.* **27,** 747–751.

Smith, M. R., Fernandes, J., Go, Y. M., and Jones, D. P. (2017). Redox dynamics of manganese as a mitochondrial life-death switch. *Biochem. Biophys. Res. Commun.* **482,** 388–398.

Soltow, Q. A., Strobel, F. H., Mansfield, K. G., Wachtman, L., Park, Y., and Jones, D. P. (2013). High-performance metabolic profiling with dual chromatography-Fourier-transform mass spectrometry (DC-FTMS) for study of the exposome. *Metabolomics* **9,** 132–S143.

Stevens, P. R., Gawryluk, J. W., Hui, L., Chen, X., and Geiger, J. D. (2014). Creatine protects against mitochondrial dysfunction associated with HIV-1 Tat-induced neuronal injury. *Curr. HIV Res.* **12,** 378–387.

Swanson, C. J., Bures, M., Johnson, M. P., Linden, A. M., Monn, J. A., and Schoepp, D. D. (2005). Metabotropic glutamate receptors as novel targets for anxiety and stress disorders. *Nat. Rev. Drug Discov.* **4,** 131–144.

Takeda, A. (2003). Manganese action in brain function. *Brain Res. Brain Res. Rev.* **41,** 79–87.

Tamanna, N., and Mahmood, N. (2014). Emerging roles of branched-chain amino acid supplementation in human diseases. *Int. Sch. Res. Notices* **2014,** 235619.

Treiman, D. M. (2001). GABAergic mechanisms in epilepsy. *Epilepsia* **42**(Suppl. 3)**,** 8–12.

Uppal, K., Soltow, Q. A., Strobel, F. H., Pittard, W. S., Gernert, K. M., Yu, T., and Jones, D. P. (2013). xMSanalyzer: Automated pipeline for improved feature detection and downstream analysis of large-scale, non-targeted metabolomics data. *BMC Bioinformatics* **14,** 15.

Uppal, K., Walker, D. I., and Jones, D. P. (2017). xMSannotator: An R package for network-based annotation of high-resolution metabolomics data. *Anal. Chem.* **89**, 1063–1067.

Uppal, K., Walker, D. I., Liu, K., Li, S., Go, Y. M., and Jones, D. P. (2016). Computational metabolomics: A framework for the million metabolome. *Chem. Res. Toxicol.* **29,** 1956–1975.

Walker, D. I., Uppal, K., Zhang, L., Vermeulen, R., Smith, M., Hu, W., Purdue, M. P., Tang, X., Reiss, B., Kim, S., *et al.* (2016). High-resolution metabolomics of occupational exposure to trichloroethylene. *Int. J. Epidemiol.* **45,** 1517–1527.

Wang, F., Franco, R., Skotak, M., Hu, G., and Chandra, N. (2014). Mechanical stretch exacerbates the cell death in SH-SY5Y cells exposed to paraquat: Mitochondrial dysfunction and oxidative stress. *Neurotoxicology* **41,** 54–63.

Wang, X., Mu, X., Zhang, J., Huang, Q., Alamdar, A., Tian, M., Liu, L., and Shen, H. (2015). Serum metabolomics reveals that arsenic exposure disrupted lipid and amino acid metabolism in rats: A step forward in understanding chronic arsenic toxicity. *Metallomics* **7,** 544–552.

Williams, A. C., Levine, R. A., Chase, T. N., Lovenberg, W., and Calne, D. B. (1980). Cfs hydroxylase cofactor levels in some neurological diseases. *J. Neurol. Neurosurg. Psychiatry* **43,** 735–738.

Wishart, D. S., Jewison, T., Guo, A. C., Wilson, M., Knox, C., Liu, Y., Djoumbou, Y., Mandal, R., Aziat, F., Dong, E., *et al.* (2013). HMDB 3.0–The human metabolome database in 2013. *Nucleic Acids Res.* **41,** D801–D807.

Xia, J., and Wishart, D. S. (2016). Using MetaboAnalyst 3.0 for comprehensive metabolomics data analysis. *Curr. Protoc. Bioinformatics* **55,** 14 10 11–14 10 91.

Xu, C. J., Klunk, W. E., Kanfer, J. N., Xiong, Q., Miller, G., and Pettegrew, J. W. (1996). Phosphocreatine-dependent glutamate uptake by synaptic vesicles. A comparison with atp-dependent glutamate uptake. *J. Biol. Chem.* **271,** 13435–13440.

Yu, T., Park, Y., Johnson, J. M., and Jones, D. P. (2009). apLCMS–adaptive processing of high-resolution LC/MS data. *Bioinformatics* **25,** 1930–1936.

Zhang, H. T., Mi, L., Wang, T., Yuan, L., Li, X. H., Dong, L. S., Zhao, P., Fu, J. L., Yao, B. Y., and Zhou, Z. C. (2016). PINK1/Parkin-mediated mitophagy play a protective role in manganese induced apoptosis in SH-SY5Y cells. *Toxicol. In Vitro* **34,** 212–219.

Zhang, S., Fu, J., and Zhou, Z. (2004). In vitro effect of manganese chloride exposure on reactive oxygen species generation and respiratory chain complexes activities of mitochondria isolated from rat brain. *Toxicol. In Vitro* **18,** 71–77.

Zhu, W., Wang, D., Zheng, J., An, Y., Wang, Q., Zhang, W., Jin, L., Gao, H., and Lin, L. (2008). Effect of (R)-salsolinol and N-methyl-(R)-salsolinol on the balance impairment between dopamine and acetylcholine in rat brain: Involvement in pathogenesis of Parkinson disease. *Clin. Chem.* **54,** 705–712.